IRIS AperTO

UNIVERSITÀ DEGLI STUDI DI TORINO

AperTO - Archivio Istituzionale Open Access dell'Università di Torino

Local Proton Source in Electrocatalytic CO2 Reduction with [Mn(bpy–R)(CO)3Br] Complexes

This is a pre print version of the following article:

Original Citation:

Availability:

This version is available http://hdl.handle.net/2318/1633130 since 2017-05-11T16:26:36Z

Published version:

DOI:10.1002/chem.201605546

Terms of use:

Open Access

Anyone can freely access the full text of works made available as "Open Access". Works made available under a Creative Commons license can be used according to the terms and conditions of said license. Use of all other works requires consent of the right holder (author or publisher) if not exempted from copyright protection by the applicable law.

(Article begins on next page)

20 August 2022

Local Proton Source in the Electrocatalytic CO_2 Reduction by Mn(bpy-R)$(CO)_3$Br Complexes

Federico Franco[a]$, Claudio Cometto[a,c]$, Luca Nencini[a]$, Claudia Barolo[a], Fabrizio Sordello[a], Claudio Minero[a], Jan Fiedler[b], Marc Robert[c], Roberto Gobetto*[a] and Carlo Nervi*[a]

Abstract: The electrochemical behavior of *fac*-[Mn(pdbpy)$(CO)_3$Br] (pdbpy = 4-phenyl-6-(phenyl-2,6-diol)-2,2'-bipyridine), **1**, in acetonitrile under Ar and its catalytic performances for CO_2 reduction with added water, 2,2',2''-trifluoroethanol (TFE) and phenol are discussed in detail. Preparative-scale electrolysis experiments, carried out at –1.5 V *vs.* SCE in CO_2-saturated acetonitrile solutions, reveal that the process selectivity is extremely sensitive to the acid strength, providing CO and formate in different faradaic yields. A detailed spectroelectrochemical (IR and UV-Vis) study under Ar and CO_2 atmospheres shows that **1** undergoes fast solvolysis; however dimer formation in acetonitrile is suppressed, providing an atypical reduction mechanism in comparison with other reported Mn^I catalysts. Spectroscopic evidence of Mn hydride formation supports the existence of different electrocatalytic CO_2 reduction pathways. Furthermore, a comparative investigation performed on the new *fac*-[Mn(ptbpy)$(CO)_3$Br] (ptbpy = 4-phenyl-6-(phenyl-3,4,5-triol)-2,2'-bipyridine) catalyst, **2**, bearing a bipyridyl derivative with OH groups in different positions to those in **1**, provides complementary information about the role that the local proton source plays during the electrochemical reduction of CO_2.

Introduction

The electrochemical conversion of carbon dioxide into value-added chemicals mediated by transition metal complexes has attracted growing interest in recent years.[1-2] The rational design of molecular catalysts that possess low overpotentials for the selective conversion of CO_2 is a crucial target, while knowledge of the main factors affecting this process will provide the basis for future improvements and advances in this field. Many organometallic catalysts have been found to selectively reduce CO_2 into such two-electron products as CO and HCOOH in non-aqueous systems. The former is widely used in mixtures with H_2 (syngas) in large-scale industrial processes.[3] Liquid solutions of formic acid can instead be directly used in green technologies (fuel cells),[4] or as hydrogen storage materials.[5] However, most of the reported homogeneous catalysts for CO_2 electrochemical reduction are selective towards CO formation,[2,6] whereas only a few of them give formate in high yields.[7]

[a] Dr. F. Franco, C. Cometto, L. Nencini, Prof. Dr. C.Barolo, Dr. F. Sordello, Prof. Dr. C. Minero, Prof. Dr. C. Nervi and Prof. Dr. R. Gobetto.
University of Turin, Department of Chemistry and NIS, Via P. Giuria 7, 10125 Turin, Italy, E-mail: carlo.nervi@unito.it
$ These authors equally contributed.
[b] Ing. CSc. J.Fiedler,
Heyrovský Institute of Physical Chemistry of ASCR, v.v.i., Dolejškova 3, 18223 Prague, Czech Republic
[c] Prof. Dr. M. Robert., C. Cometto
Univ. Paris Diderot, Sorbonne Paris Cité, UMR CNRS 7591, Laboratoire Electrochimie Moléculaire, F-75205 Paris 13, France

Supporting information for this article is given via a link at the end of the document.

fac-[M(bpy-R)$(CO)_3$X] (M = Mn^I, Re^I; bpy-R = 2,2'-bipyridine-based ligands; X = Cl^- or Br^-) complexes have been widely studied as precursors to efficient electrocatalysts for the reduction of CO_2 to CO. In particular, Mn complexes bearing 4,4'-disubstituted bipyridines with H, CH_3 and *t*-Bu (since all complexes herein mentioned are *fac*- we will omit this label) are valid low-cost alternatives to the Re^I counterparts in terms of stability, selectivity and efficiency.[8] The combination of IR/UV-Vis spectroelectrochemistry (SEC)[9] with non-conventional spectroscopic techniques[10-12] and computational methods,[13] provided valuable complementary tools to electrochemistry for elucidating the electrocatalytic mechanism of CO_2 reduction by Group VII metal based catalysts. These studies suggest that doubly reduced pentacoordinated species [M(bpy-R)$(CO)_3]^-$ (M = Mn, Re) are responsible for the catalytic conversion of CO_2 into CO. Nevertheless, there are several differences in the electrocatalytic behavior of the two classes of complexes. The Mn catalysts are formed upon the reductive cleavage of the [Mn(bpy-R)$(CO)_3]_2$ dimer, which is generated after the 1e reduction of the starting species and subsequent rapid dissociation of the halogen ion. Contrariwise, the structurally similar [Re(bpy-R)$(CO)_3]_2$ dimer is known to be a side-product in the electrocatalytic cycle of Re complexes.[14] In an effort to reduce the overpotential required for the formation of the catalytically active species, Kubiak and coworkers have recently exploited the bulky nature of the mesbpy ligand (6,6′-dimesityl-2,2′-bipyridine) to prevent dimerization in [Mn(mesbpy)-$(CO)_3$Br].[15] However, the [Mn(mesbpy)$(CO)_3$(COOH)] adduct requires a third "extra-electron" and catalysis occurs more negatively even though the [Mn(mesbpy)$(CO)_3]^-$ anion is formed via a 2e transfer (ECE mechanism) at less negative potentials than in the case of bpy. Moreover, unlike the polypyridyl Re catalysts, Mn-based catalytic CO_2 conversion is commonly observed only in the presence of an added proton source (water, methanol or TFE).[8,15] Nevertheless, we have recently reported the first case of a bromotricarbonyl Mn^I catalyst, namely [Mn-(pdbpy)$(CO)_3$Br] (**1**) that is capable of reducing CO_2 even in *anhydrous* acetonitrile,[16] without the need for deliberate addition of Brønsted acids.[17] This unique behavior has been ascribed to the structure of the pdbpy ligand, in which the pendant phenolic groups near to the metal center may act as intramolecular proton sources (Figure 1). We found that the presence of local protons not only provided a dramatic enhancement in the electrocatalytic activity towards CO_2 reduction, but also an unexpected change in selectivity, producing a non-negligible amount of formate in addition to CO. Two distinct pathways have therefore been proposed along with the formation of an electroinduced Mn hydride species, which was assumed to be responsible for $HCOO^-$ production, as reported in recent photocatalytic studies on [Mn(bpy)$(CO)_3$Br].[18,19]

Encouraged by the remarkable electrocatalytic activity of **1** under CO_2, we firstly aimed to in-depth investigate its unusual electrochemical behavior under inert atmosphere by using cyclic voltammetry (CV) and IR/UV-Vis SEC.

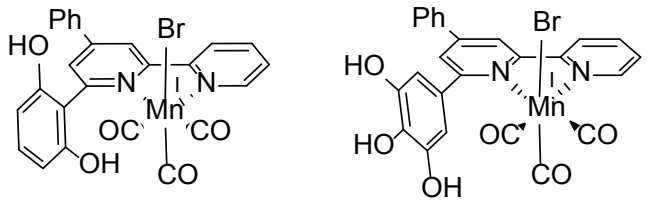

$Mn^{I}(pdbpy)(CO)_3Br$ (**1**) $Mn^{I}(ptbpy)(CO)_3Br$ (**2**)

Figure 1. Chemical sketches of the complex **1** and **2**.

Furthermore, the effect due to the addition of different proton sources (H_2O, TFE and phenol) on either the electrocatalytic activity and selectivity of **1** under CO_2 was also evaluated. Finally, a comparative study on the structurally similar [Mn(ptbpy)$(CO)_3$Br] (**2**), containing three local OH groups in *meta* and *para* positions of the phenolic ring in 6, *i.e.* a little farther from the Mn center than in **1** (Figure 1), provided further useful information to better understand the role of an intramolecular proton source on the electrochemical and electrocatalytic properties of this class of catalysts.

Results and Discussion

Synthesis and characterization. The pdbpy and ptbpy ligands were synthesized using the Kröhnke reaction and by coupling the corresponding pyridinium iodides and chalcones according to the reported procedure.[17] A demethylation reaction, based on refluxing the precursor in a CH_3COOH solution of HBr (33%), was used to synthesize the final ptbpy ligand. Full details can be found in the Experimental Section.

Cyclic voltammetry (CV) under Ar. CV of complex **1** in MeCN under inert atmosphere[17] exhibits three consecutive reduction waves (Figures 2 and S1). The first two reduction processes, R1 and R2, are chemically irreversible (E_p = –1.21 V, –1.50 V *vs.* SCE), whereas the third reduction R3 appears to be quasi-reversible ($E_{1/2}$ = –1.66 V). R2 and R3 current peaks decrease with respect to R1 (Figure S2) upon increasing the scan rate. This is consistent with a mechanism in which chemical processes following R1 generate the species undergoing the reductions R2 and R3.

As we will discuss later, the SEC experiments performed under Ar highlighted two key aspects that strongly influence the electrochemical behavior of **1** in MeCN. First of all, rapid solvolysis of the Mn-Br bond even occurs at open circuit in the dark at room temperature. This behavior has been reported for similar complexes.[20-21] Solutions of **1** in MeCN are thus mixtures of **1** and the positively charged $[Mn(pdbpy)(CO)_3(MeCN)]^+$ (**1a**). Moreover, the dimerization of **1** was not spectroscopically detected by IR and UV-Vis SEC upon R1 (see below). This is in agreement with CV, where no anodic reoxidation peak of the dimer, commonly found at around –0.3 V,[8] is observed (Figure S1). Thus, the first reduction is chemically irreversible, but no dimer is formed. Exhaustive experiments under Ar performed just after R1 (–1.25 V vs. SCE) consumed one electron per molecule of **1**. More information about the chemical processes involved in the course of R1 will be given below.

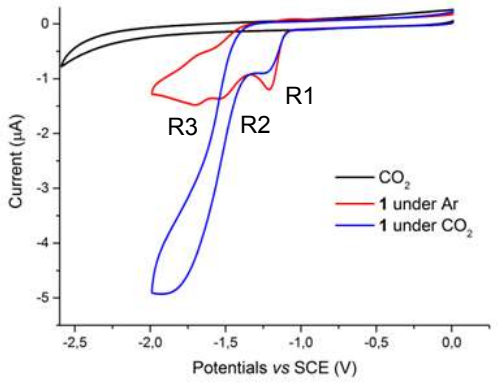

Figure 2. CVs of a MeCN solution of **1** (0.5 mM) at 100 mV s^{-1} under Ar (red curve) and CO_2 (blue curve), at a glassy carbon electrode. The black line is the CO_2-saturated blank.

Conversely, CV of **2** in MeCN under Ar significantly differs from that of **1** (Figure 3), resembling that of the well-known [Mn(bpy)$(CO)_3$Br].[8] It exhibits a first irreversible reduction, R1', at E_p = -1.30 V, followed by fast Br^- dissociation and the subsequent formation of the Mn-Mn dimer, which is then reoxidized at -0.49 V (O1', Figure 3). As evidenced by the IR-SEC data (see below) the replacement of Br^- by MeCN at open circuit is much slower in **2**.

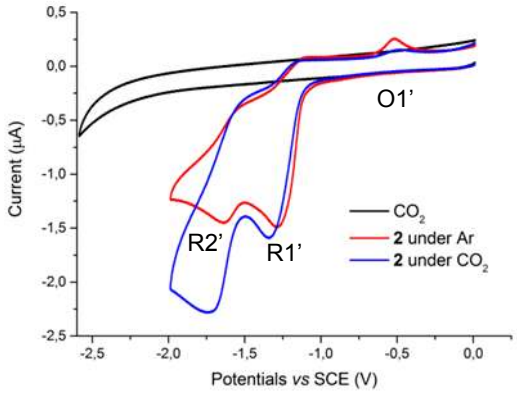

Figure 3. CVs of a MeCN solution of **2** (0.5 mM) at 100 mV s^{-1} under Ar (red curve) and CO_2 (blue curve), at a glassy carbon electrode. The black line is the CO_2-saturated blank.

The second irreversible reduction of **2**, R2', occurs more negatively, at E_p = -1.64 V. The relationship between the peak current of R2' and the CV scan rate is similar to findings for waves R2 and R3 in **1** (Figure S3). In a 1 mM solution the apparent single R2' peak splits into two almost overlapped

peaks that are *ca.* 70 mV separated from each other (E_p = -1.61 and -1.68 V, respectively) (Figure S4). The Mn catalyst containing the 6-(2-hydroxyphenyl)-2,2′-bipyridyl ligand showed an analogous CV response in MeCN + 5% H_2O, but the nature of the two reductions (at about -1.30 V in that case) was not explained.[22] They might be related to the presence of partially deprotonated intermediate species in solution which may be formed in the course of the reductive scan on the CV timescale. Further discussion of this point is given below.

Infrared Spectroelectrochemistry (IR-SEC) under Ar and DFT calculations of ν_{CO} stretches.

*IR-SEC of **1** in MeCN/TBAPF$_6$.* IR-SEC experiments were performed in an OTTLE cell in order to get further insights about the reduction paths of **1** and **2**. This technique has already been used to characterize key intermediates during the electrochemical reduction of carbonyl organometallic electrocatalysts by monitoring the spectral changes of the CO stretching bands, ν_{CO}.[9] DFT calculations were employed as an additional tool to support the assignment of the intermediate species observed during the IR-SEC experiments.

Table 1. Selected experimental and calculated ν_{CO} in MeCN.

Complex[]	Experimental	DFT[]
[Mn(pdbpy)(CO)$_3$Br] (**1**)	2026, 1935, 1925(sh)	2013, 1939, 1928
[Mn(pdbpy)(CO)$_3$(MeCN)]$^+$ (**1a**)	2044, 1961	2033, (1962, 1951)
[Mn(pdbpy)(CO)$_3$Br]$^-$		1984, 1911, 1900
[Mn(pdbpy)(CO)$_3$(MeCN)]		2014, 1938, 1926
[Mn(pdbpy−H$^+$)(CO)$_3$] (**1b**)	2021, 1920(br)	2010, (1925, 1916)
[HMn(pdbpy−H$^+$)(CO)$_3$]$^-$ (**1c**)	1987, 1899, 1878(sh)	1972, 1891, 1879
[HMn(pdbpy)(CO)$_3$] (**1c'**)		1988, 1908, 1897
[Mn(pdbpy−H$^+$)(CO)$_3$]$^{2-}$ (**1d**)	1910, 1818(br)	1892, (1832, 1808)
[Mn(pdbpy−2H$^+$)(CO)$_3$]$^-$ (**1e**)	2012, 1916, 1900(sh)	1998, 1912, 1899
[Mn(pdbpy−2H$^+$)(CO)$_3$]$^{3-}$ (**1f**)	1910, 1805[a]	1874, (1814, 1785)
[Mn(ptbpy)(CO)$_3$Br] (**2**)	2023, 1936, 1914	
[Mn(ptbpy)-(CO)$_3$(MeCN)]$^+$ (**2a**)	2044, 1958	
[Mn(ptbpy)(CO)$_3$]$_2$ (**2b**)	1932, 1880, 1868, 1847	
[HMn(ptbpy–H$^+$)(CO)$_3$]$^-$ (**2c**)	1987	
[Mn(ptbpy)(CO)$_3$]$^-$ (**2d**)	1912, 1817, 1804[a]	
[HMn(bpy)(CO)$_3$]	1989, 1892 [a]	
[HMn(bpy)(CO)$_3$]	1991, 1892, 1888sh	1978, 1893, 1884
[Mn(CO)$_3$(bpy)]$^-$	1916,1814.5 [b]	-
[Mn(CO)$_3$(bpy)]$^-$	1911, 1811	1890, (1816, 1812)

[a] THF as solvent, data from ref. [24] ; [b] THF as solvent, data from ref. [9a]

Tables 1 and S1 summarize the experimental and DFT calculated infrared data for all the transient species proposed here, together with those reported for similar Mn complexes in the literature. In *dry* acetonitrile and before applying any potentials, **1** shows two different sets of three ν_{CO}, which are both typical of facially coordinated [Mn(bpy-R)(CO)$_3$X] complexes (Figure S5*a*). This is a clear indication[20-21] that the axial Br^- in **1** is replaced by the solvent even in the dark and at room temperature. Thus, the IR spectra of MeCN solutions of **1** exhibit mixtures of the original Br^- containing complex (ν_{CO} bands at 2026, 1935, 1925sh cm^{-1}) and the MeCN-containing cation **1a** (2044, 1961 cm^{-1}), in a time-dependent ratio due to the proceeding of the solvolysis equilibrium (Figure S5*a*). The two low-energy ν_{CO} bands of **1** overlap with those of **1a**. In a typical run, the solvent complex, **1a**, was found to be the major species at the beginning of the IR-SEC experiments (Figure S5*b*). Weaker bands at 1613 and 1623 cm^{-1} are assigned to the plane stretching of the aromatic rings (bpy and Ph modes are mixed) of **1** and **1a**, respectively. When a potential slightly more negative than R1 is applied, both the series of bands corresponding to the starting forms **1** (2026, 1935, 1925(sh), 1613 cm^{-1}) and **1a** (2044, 1961, 1623 cm^{-1}) progressively disappear, leading to growth of a new species as major reduction product with absorptions at 2021, 1920(br) (CO stretches) and 1607 cm^{-1} (ligand-based stretch mostly overlapped with those belonging to **1**) (Figure 4).

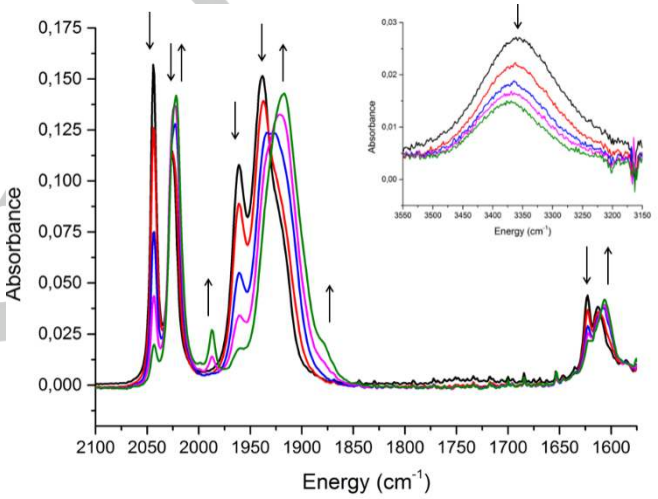

Figure 4. IR-SEC of a 1 mM MeCN solution of **1** under Ar: reduction at the first peak (R1). The inset shows a concomitant decrease of the vOH

The latter species can be reasonably assigned to a singly-deprotonated neutral species, [Mn(dhbpy−H$^+$)(CO)$_3$] (**1b**), formed by a reductive deprotonation of the starting **1a** upon R1. Accordingly to this interpretation, the newly formed bands fit well with the spectroscopic data of Re and Mn complexes that contain the 4dhbpy ligand (4,4′-dihydroxy-2,2′-bipyridyl) and in which a reductive deprotonation mechanism was reported.[21,23] In particular, a shift in the high-energy ν_{CO} from 2019 to 2012 cm^{-1} (7 cm^{-1} red shift) was observed in [Re(4dhbpy)(CO)$_3$Cl] as the starting species transformed into the singly-deprotonated complex [Re(4dhbpy−H$^+$)(CO)$_3$Cl]$^-$ (Table S1).[23] Similarly, a corresponding 5 cm^{-1} red shift is experimentally observed passing from **1** (2026 cm^{-1}) to [Mn(pdbpy−H$^+$)(CO)$_3$] **1b** (2021 cm^{-1}). This interpretation is also supported by the decrease of the broad OH stretching band at around 3359 cm^{-1} (calculated at 3363 cm^{-1}) during the first reduction (Figure 4, inset). The R1 process is also chemically irreversible in IR-SEC, since reoxidation does not restore the initial spectrum (Figure S6). From a structural point of view, DFT calculations suggest that the phenolate group in **1b** may occupy the vacant coordination position (after the release of MeCN from **1a**, Mn-O = 2.052 Å).

The interaction between the Mn^{I} center and the negatively charged phenolate unit in the axial position is expected to stabilize the pseudo-octahedral (distorted) structure of **1b**, thus accounting for the lack of dimerization upon R1. Furthermore, Mn retains its original +1 oxidation state in **1b**, maintaining a similar electron density on the $Mn(CO)_3$ moiety to that of **1** (as reflected by a very small shift in ν_{CO}). DFT ν_{CO} predictions of **1**, **1a** and **1b** well reproduce the experimental data (Table 1).

The two sets of calculated transitions at 1962/1951 cm^{-1} and 1925/1916 cm^{-1} are in good agreement with the broad experimental absorptions at 1961 and 1920 cm^{-1} for **1a** and **1b**, respectively. Finally, it is worth mentioning that the hypothetical assignment of **1b** to the neutral six-coordinate $[Mn(dhbpy{-}H^{+})(CO)_3(CH_3CN)]$ can be ruled out by the absence of any observable band in the region between the ν_{CO} stretches of **1** and **1a**, respectively, after R1.[21]

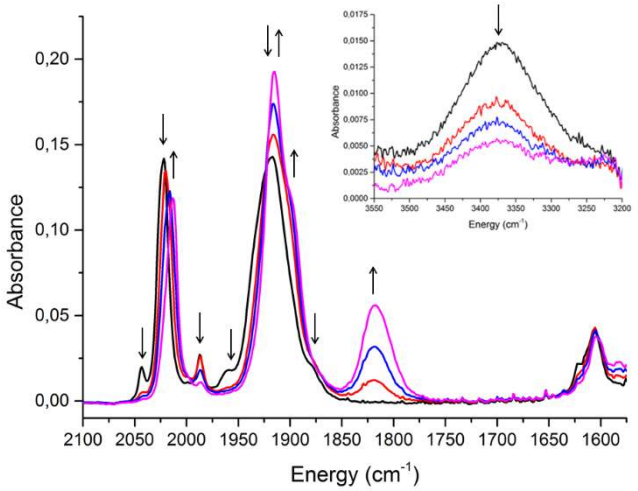

Figure 5. IR-SEC of a 1 mM MeCN solution of **1** under Ar: reduction at the second peak (R2). The inset shows further decrease of ν_{OH}.

Actually, less intense ν_{CO} at 1987 and 1878(sh) cm^{-1} appear after reduction at R1 in addition to the bands of **1b** (Figure 4). We assign these weak ν_{CO} to the Mn hydride $[HMn^{I}(pdbpy{-}H^{+})(CO)_3]^{-}$ **1c**, formed by intramolecular proton transfer from pdbpy to the metal (with a negative charge formally localized on the phenolate). Although rare cases of carbonyl Mn hydrides have been spectroscopically characterized, similar ν_{CO} were reported by Riera et al. for the analogous $[HMn^{I}(bpy)(CO)_3]$ in THF (1989 and 1892 cm^{-1}).[24] We were able to reproduce the literature data by performing the IR-SEC of $[Mn(bpy)(CO)_3Br]$ in MeCN with 0.1 M of phenol (Figure S7). The reduction of the dimer that was initially formed (ν_{CO} at 1976, 1963vw, 1933, 1879, 1857 cm^{-1}), gave the $[Mn(bpy)(CO)_3]^{-}$ anion (ν_{CO} at 1911 and 1811 cm^{-1}), which is quickly transformed into the hydride species in the presence of 0.1 M phenol (ν_{CO} at 1991, 1892, 1888sh cm^{-1}). In more acidic conditions the production of the dimer is strongly reduced and the hydride is more directly formed (Figure S7b). These data are in good agreement with our experimental and theoretical data on **1c** (Table 1).

When the cell potential is stepped more negative to R2 (~–1.5 V), decay of both species **1b** and **1c** produced upon R1 is balanced by simultaneous growth of two different sets of ν_{CO} stretches, indicating the formation of two new species (Figure 5). The ν_{CO} stretches at 1916 and 1818 cm^{-1}, which are in excellent agreement with several reported doubly-reduced five-coordinate Mn anions,[8b,9a,15] can be assigned to the partially deprotonated $[Mn(dhbpy{-}H^{+})(CO)_3]^{2-}$ anion (**1d**), which still possesses one local OH group attached to the ligand moiety. Furthermore, concomitantly to **1d** formation, a 9 cm^{-1} shift of the IR signal at 2021 cm^{-1} to lower energy indicates a partial conversion of **1b** into another species, characterized by a growing ν_{CO} stretch at 2012 cm^{-1} and a poorly resolved shoulder at 1900 cm^{-1} (Figure 5). The ligand mode at 1607 cm^{-1} of **1b** is also slightly shifted to 1605 cm^{-1}. These spectroscopic features are consistent with the doubly-deprotonated intermediate $[Mn(dhbpy{-}2H^{+})(CO)_3]^{-}$ (**1e**), derived from further reductive deprotonation of **1b** and structurally similar to the latter. This interpretation is in accordance with further decrease of the ν_{OH} stretch at 3359 cm^{-1}, which is experimentally seen during R2 in the recorded spectra (Figure 5, inset). Moreover, an analogous red-shift (~10 cm^{-1}) of the high energy ν_{CO} stretch was reported for the reductive conversion of the related complex $[Re(4dhbpy{-}H^{+})(CO)_3Cl]^{-}$ to the doubly-deprotonated $[Re(4dhbpy{-}2H^{+})(CO)_3]^{-}$ (Table S1).[23] The DFT calculated ν_{CO} stretches match well with the experimental ones, for either **1d** (1892, 1832, 1808 cm^{-1}) and **1e** (1998, 1912, 1899 cm^{-1}).

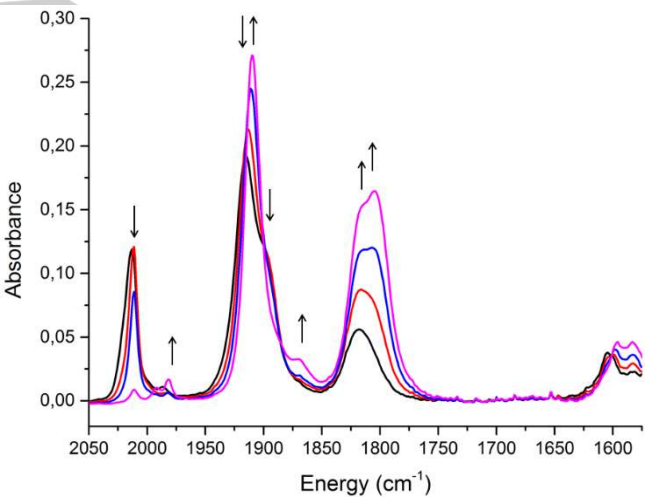

Figure 4. IR-SEC of a 1 mM MeCN solution of **1** under Ar: reduction at the third peak (R3).

The ν_{CO} at 2012 and 1900 cm^{-1} disappear at slightly more negative potentials, while ν_{CO} centered at 1910, 1817 and 1805 cm^{-1} appear (Figure 6). The net result is that the IR spectrum at the end of the reduction shows a very intense sharp ν_{CO} at 1910 cm^{-1} and a broader one, split into two maxima at 1817 and 1805 cm^{-1}, respectively. These spectral changes likely indicate that the **1d** anion coexists with its deprotonated counterpart $[Mn(pdbpy{-}2H^{+})(CO)_3]^{3-}$ (**1f**) in solution, resulting from the reduction of **1e**. **1d** and **1f** share the same five-coordinate geometry as the $[Mn(bpy\text{-}R)(CO)_3]^{-}$ species, as suggested by the similarity in their IR features (see Table 1).[8b,9a,15] It should

be also mentioned that direct interconversion between **1d** and **1f** via acid-base equilibria in solution is non-negligible due to the pH-dependent properties of the pdbpy ligand. For this reason, it is hard to clearly distinguish the differently protonated anionic forms in the experimental IR spectra.[21] These chemical complications, as well as the highly reducing potentials, probably contribute to the appearance of some minor Mn species in the final spectrum, characterized by very weak ν_{CO} bands (*e.g.* at 1982 and 1869 cm^{-1}, Figure 6).

IR-SEC of **2** *in* $CH_3CN/TBAPF_6$. As preliminarily suggested by CV data, an IR-SEC study of **2** confirmed the remarkable differences in the reduction mechanism with respect to **1**, highlighting the crucial role played by the local proton source. The solvolysis equilibrium in **2** is less marked than in **1**, so that the IR spectrum of a MeCN solution of **2** shows three main ν_{CO} at 2023, 1936 and 1914 cm^{-1}, corresponding to the Br-containing initial form. However, bands at 2044 and 1958 cm^{-1} (Figure S8) rapidly grow just before the first reduction, suggesting that the cationic $[Mn(ptbpy)(CO)_3(CH_3CN)]^+$ (**2a**) complex is rapidly generated by a catalytic ETC (electron transfer chain) reaction.[25]

Upon the first reduction R1', decrease in the ν_{CO} of **2** (2023, 1936, 1914 cm^{-1}) and **2a** (2044, 1958 cm^{-1}) is balanced by the growth of ν_{CO} at 1932, 1880, 1868 and 1847 cm^{-1}, likely corresponding to the dimer $[Mn(ptbpy)(CO)_3]_2$ (**2b**) (Figure 7).

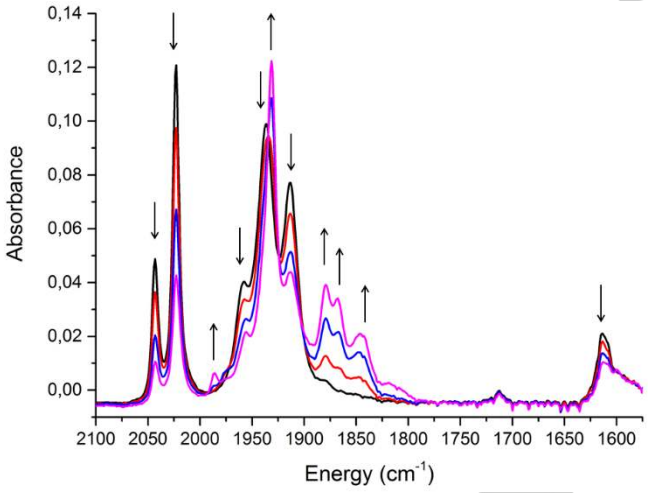

Figure 5. IR-SEC of a 1 mM MeCN solution of **2** under Ar: reduction at the first peak (R1').

This interpretation matches not only with the CV data of **2**, but also with the experimental IR-SEC data reported for analogous systems.[9a,12] A small peak at 1987 cm^{-1} also grows during R1', indicating the partial formation of a Mn hydride species ($[HMn(ptbpy{-}H^+)(CO)_3]^-$, **2c** (or protonated counterparts). Consistently with a less spatial interaction between the intramolecular phenolic groups and the metal atom in **2**, it is apparent that the hydride **2c** is generated *in-situ* in a considerably smaller amount than the analogue **1c**.

At increasingly negative potential values, the ν_{CO} of the dimer decrease, while the very intense ν_{CO} at 1912, 1817 and 1804 cm^{-1} start to increase (Figure 8). These spectral changes are consistent with a reductive cleavage of the dimer to generate the five-coordinate $[Mn(ptbpy)(CO)_3]^-$ (**2d**) anion. The similarity between the IR spectrum shown in Figure 8 and the one obtained after the IR-SEC experiment on **1** (Figure 6), prompted us to assign the increasing bands at 1912, 1817 and 1804 cm^{-1} to a mixture of differently protonated anionic species (mostly derived from acid-base processes).

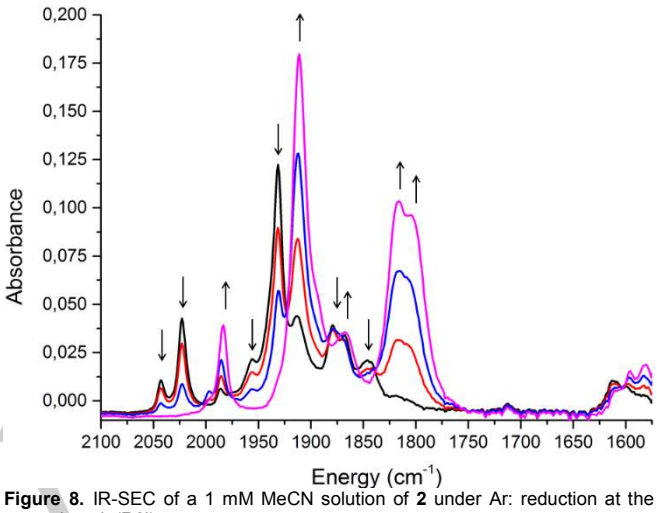

Figure 8. IR-SEC of a 1 mM MeCN solution of **2** under Ar: reduction at the second peak (R2').

UV-Vis Spectroelectrochemistry (UV-Vis SEC) under Ar. In the OTTLE cell, at open circuit, the UV-Vis spectrum of **1** in MeCN shows a series of absorptions at 382, 283(sh), 273 and 250 nm (FigureS9a), which do not undergo any appreciable changes during the electrochemical reduction R1. This is consistent with the formation of **1b** upon R1, as the theoretical UV-Vis spectra of **1a** and **1b** (Figure S10) resulted to be very similar to each other. Importantly, the absence of any intense absorption at around 800 nm confirmed the lack of dimerization after R1, as already evidenced by the electrochemical and IR-SEC results.[8a,9a] When the applied potential is close to R2 (*ca.* –1.5 V), a broad absorption at 627 nm and other minor bands at 375, 243 nm start to grow to the detriment of the maxima at 283, 273, 250 nm (Figure S9b), indicating the formation of a five-coordinate anion, analogous to $[Mn(bpy)(CO)_3]^-$ produced upon 2e reduction of $[Mn(bpy)(CO)_3Br]$ in MeCN.[8a] At slightly more negative potentials, the band at 243 nm decreases, with an isosbestic point at 290 nm, while a new, intense band appears at 506 nm and the maximum at 627 nm is slightly blue-shifted to 622 nm (Figure S9c). These spectral changes are in agreement with the formation of a mixture of analogous pentacoordinated Mn species after R3.[8a]

Proposed reduction mechanisms under Ar. The set of experimental data in MeCN led us to propose two different reduction routes for **1** (Scheme 1) and **2** (Scheme 2). A rational understanding of the reduction pathway for **1** should take into account the solvolysis process which provides an initial mixture of **1** and **1a**. Since it seems reasonable to assume that the reduction of **1a** occurs more positively than **1** and IR-SEC clearly

showed that **1a** is thermodynamically favored over **1**, we will consider R1 simply describing the 1e reduction of **1a**. As evidenced by IR-SEC, chemical complications interfere with the redox process occurring at R1, yielding the neutral **1b** species as the major product via a reductive deprotonation of **1a** (after release of a solvent molecule).

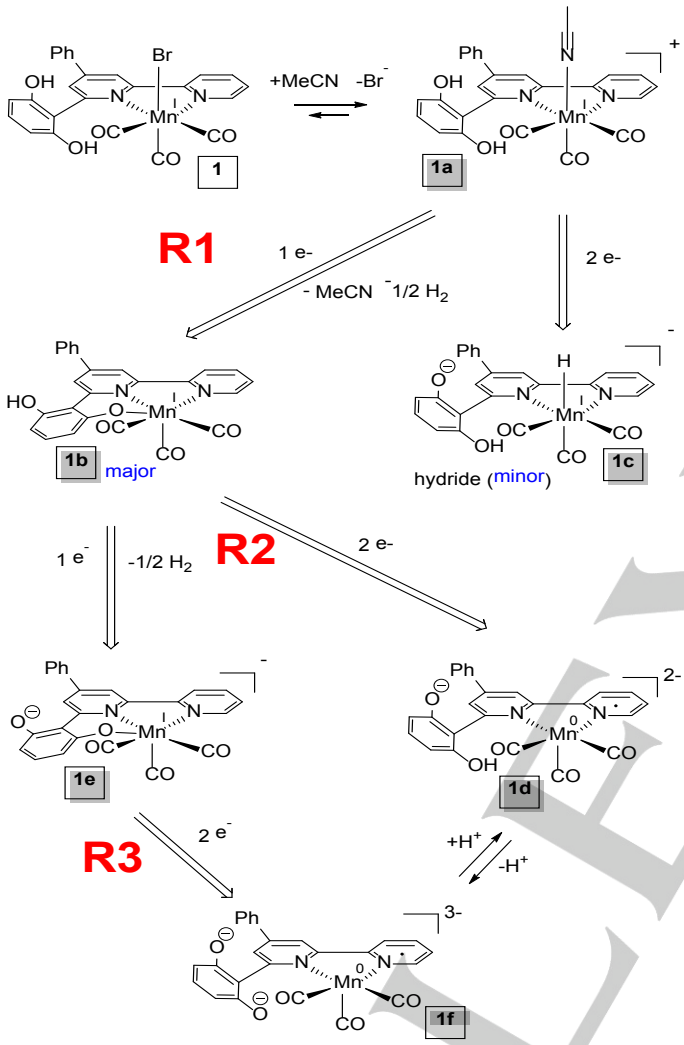

Scheme 1. Electrochemical mechanism for **1** under Ar.

As discussed above, reductive deprotonation is not uncommon in Group VII carbonyl complexes containing pyridinol moieties.[21,23] No experimental evidence of dimerization after R1 was obtained. However, a small amount of the hydride **1c** was detected by IR-SEC at this reduction potential. Formally, it should be produced via an overall two electron reduction, but electrolysis (at longer timescale than SEC) apparently consumed only one electron per molecule of **1**. By the way, as suggested by DFT calculations, the reactions of **1c** with the starting complexes **1** or **1a** leading to **1b** are thermodynamically spontaneous (ΔG = –103.7 kJ/mol for **1c** + **1** → 2 **1b** + H_2 + Br^- and ΔG = –110.7 kJ/mol for **1c** + **1a** → 2 **1b** + H_2 + MeCN), thus accounting for the overall consumption of one electron per molecule of **1b** produced.

At the onset potential of R2, **1b** is reduced into a transient radical species (not experimentally observed), which undergoes two competing chemical processes. Firstly, as an effect of increasing negative charge over the diimine moiety, the axial phenolate coordination to Mn becomes more labile in the reduced form of **1b**, promoting dissociation of the Mn-O bond. Upon R2, the resulting species further reduces to produce the doubly-reduced, singly-deprotonated anion **1d**. In parallel, the aforementioned short-lived radical species may undergo another reductive deprotonation, providing the doubly-deprotonated intermediate **1e**. The net result is that, as observed by IR-SEC, **1d** and **1e** coexist at the potential of R2 (Figure 5). The electrochemical conversion of **1e** into **1f** is analogue to the conversion of **1b** into **1d**. The proposed mechanism is also in agreement with the voltammetric behavior of **1** at different scan rates (Figure S2).

The electrochemical behavior of **2** under Ar is straightforward (Scheme 2), and similar to other [Mn(diimine)$(CO)_3$X] complexes, where the formation of the dimer **2b** is the only relevant process experimentally observed upon the first 1e reduction (R1'). The hydride **2c**, albeit detected in IR-SEC, is produced only in very small amount, if compared with **1c**. Unlike **1**, CV and IR-SEC gave no indication of deprotonation during the first reduction of **2**. In the subsequent reduction, R2', the reductive cleavage of **2b** produces the pentacoordinated anion **2d** (or a mixture of differently protonated anions).

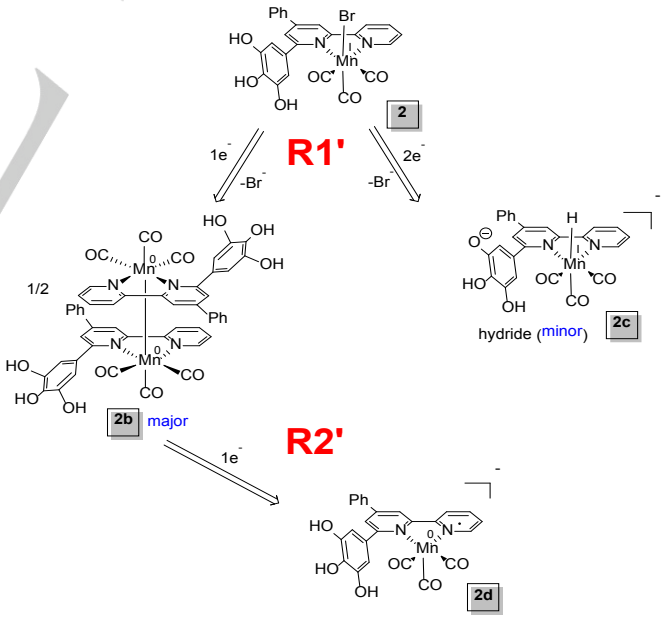

Scheme 2. Electrochemical mechanism for **2** under Ar.

Catalytic behavior under CO_2. To investigate the catalytic process, we performed IR-SEC on a MeCN/$TBAPF_6$ solution of **1** under CO_2-saturated conditions. During the first reduction, where no catalytic current in CV was observed, the recorded spectra are similar to those obtained under Ar, as the

consumption of the starting species **1** and **1a** gives the catalytically inactive neutral intermediate **1b**, with typical ν_{CO} at 2021, 1918 cm^{-1} and the ligand-based absorption at 1607 cm^{-1} (Figure S12). Interestingly, the characteristic ν_{CO} of **1c** are not observed at R1 and are replaced by growth of new bands in the 1700-1500 cm^{-1} region of the FTIR spectra. This seems to suggest that either the Mn hydride **1c** or its radical precursor may interact with the substrate. Unfortunately this new set of ν_{CO} cannot be univocally assigned to CO_2 reduction products (*e.g.* free $HCOO^-$) or to a Mn-CO_2 adduct due to partial overlap with the bands of **1b**,[15,26] so that we cannot rule out the formation of a new *fac*-tricarbonyl Mn^I-CO_2 complex, as found for an analogous Mn^I and Re^I catalysts.[15,23,26,29] Besides this, the asymmetric ν_{COO} stretches of such adducts (between 1700-1600 cm^{-1}) would also completely overlap with those of HCO_3^-/CO_3^{2-}.[9b,27] In agreement with the CV data, the catalytic CO_2 reduction process starts at more negative potentials than R1, as suggested by an evident decay of the CO_2 signal at 2342 cm^{-1} (asymmetric stretching mode). In the ν_{CO} region the high-energy band of **1b** is slightly shifted to 2019 cm^{-1}, whereas the broad absorption at 1918 cm^{-1} is slowly replaced by two different ν_{CO} at 1921 and 1907 cm^{-1} (Figure S13). The recorded IR spectra do not change significantly once these three bands are fully grown up, as expected for the proceeding of a typical catalytic run. No bands around 1800 cm^{-1} related to the anions **1d** or **1f**, considered catalytically active for CO production, were observed (Figure S13). At the same time, the rapid increase of the band at 1607 cm^{-1}, which is partially overlapped with the bpy-based mode of **1b**, gives a clear indication of the electrocatalytic formation of free formate.[9b,27] This is in agreement with the results of the bulk electrolysis performed on **1** under CO_2 in dry MeCN.[17] Moreover, two other bands, increasing at 1684 and 1646 cm^{-1}, can be assigned to free bicarbonate,[9b,9d,27] and are often related to catalytic CO production. Finally, as previously observed,[28] evolution of gas on the working electrode surface and a small rising peak, caused by CO adsorbed on Pt, was seen at 2138 cm^{-1}. The band at 1646 cm^{-1} may result from the overlap with that of the carbonate ion (as an ion pair), since it appears to grow independently of the signal at 1684 cm^{-1}.[9b,29] At lower CO_2 concentrations, the three ν_{CO} at 2019, 1921 and 1907 cm^{-1} are isosbestically converted into a mixture of **1d** and **1e** only after the consumption of approximately 50% of the starting CO_2 (Figure S14).

Analogously to **1**, CV of the complex **2** in a CO_2 saturated MeCN solution exhibits an increased peak current upon the second reduction R2' (at –1.50 V, Figure 3), even though the observed electrocatalytic current enhancement is much lower in comparison to **1** under the same conditions (Figure 2). Accordingly with the electrochemical data, no catalytic process is observed after the first reduction in IR-SEC in a CO_2-saturated MeCN solution of **2** (Figure S15), but the dimer **2b** is quantitatively produced from the starting **2** and **2a**. However, as previously discussed for **1**, the small ν_{CO} at 1987 cm^{-1}, assigned to the Mn hydride **2c**, is no longer detected during reduction under CO_2. As in **1**, a catalytic behavior is observed at the foot of the second reduction, showing a growth of bands at 1684, 1646 (free HCO_3^-/CO_3^{2-}) and 1607 (free formate) cm^{-1} concomitantly to a decrease of the CO_2 stretching mode at 2342 cm^{-1} (Figure S16). Nevertheless, the detection of **2d** even under CO_2-saturated conditions confirms the reduced catalytic activity of **2** in comparison with **1**. Furthermore, growth of the IR signal at 1607 cm^{-1} during catalytic CO_2 reduction is less evident than in the case of **1**. This may suggest a slower formation of the hydride species, believed to be responsible for catalytic CO_2 conversion into formate, and is consistent with a more difficult intramolecular H^+ transfer for **2**.

Electrolysis under CO_2 in the presence of Brønsted acids. The catalytic performances of **1** and **2** were also investigated in the presence of different Brønsted acids. In particular, water, TFE or phenol (2.7 M) were added to MeCN solutions (0.5 mM) of **1** and **2**. Bulk electrolysis was performed at –1.50 V (for 2h) and –1.70 V (for 3h with water and phenol and for 50 min with TFE), for **1** and **2**, respectively. Table 2 summarizes the quantitative results obtained during the exhaustive experiments.

Table 2. TON and faradic efficiencies (η) from bulk electrolysis (applied potentials E in V *vs.* SCE) of a 0.1 M $TBAPF_6$ MeCN solutions of **1** and **2** (0.5 mM) in the presence of different Brønsted acids (2.7 M).

Catalyst	E (V)	Time (min)	Acid (2.7 M)	TON			(η %)		
				CO	$HCOO^-$	H_2	CO	$HCOO^-$	H_2
1	–1.50	120	H_2O	28	1.4	0.7	90	4	2
	–1.50	120	TFE	11	9	0.8	48	36	3
	–1.50	120	phenol	4	12	5.5	15	39	21
2	–1.70	180	H_2O	7	0.5	0.2	74	4	2
	–1.70	50	TFE	2	0.3	0.04	74	10	1
	–1.70	180	phenol	2	0.8	0.9	56	15	17

A CO_2 flow of 50 mL min^{-1} was kept constant during the experiments, whereas gaseous and liquid CO_2 reduction products were determined by gas (GC) and ion (IC) chromatography, respectively. CVs carried out on solutions of **1** and **2** in the presence of H_2O show a significant catalytic current enhancement under CO_2 (Figure 9a), which is in agreement with previously reported Mn catalysts. Notably, the catalytic currents observed for **1** at the peak potentials of R2 and R3, in aqueous MeCN under CO_2, are considerably higher than the peak current achieved under an inert atmosphere at the same potentials, indicating that **1** is able to efficiently and selectively reduce CO_2, even in the presence of a considerable amount of water (Figure 9a). In this case the wave seems to have reached a plateau, so that we can roughly estimate the catalytic rate constant, k_{cat},[30] equal to 81 s^{-1}. An analogous selective catalytic mechanism for CO_2 reduction is expected also for **2**, being characterized however by a considerably lower catalytic current under CO_2 (Figure 9b).

Bulk electrolysis experiments on CO_2-saturated aqueous MeCN solutions well reproduce the CV data, revealing selective CO production. In particular, faradaic efficiencies η_{CO} of 90% and 74% with TON_{CO} of 28 and 7 were found for **1** and **2**, respectively (Figure S17a-b). Conversely, the competing catalytic processes that yield $HCOO^-$ and H_2 are almost

suppressed, providing η_{HCOO} = 4% (TON_{HCOO} of 1.4 for **1** and 0.5 for **2**) and η_{H2} = 2% (TON_{H2} of 0.7 for **1** and 0.2 for **2**) for both catalysts.

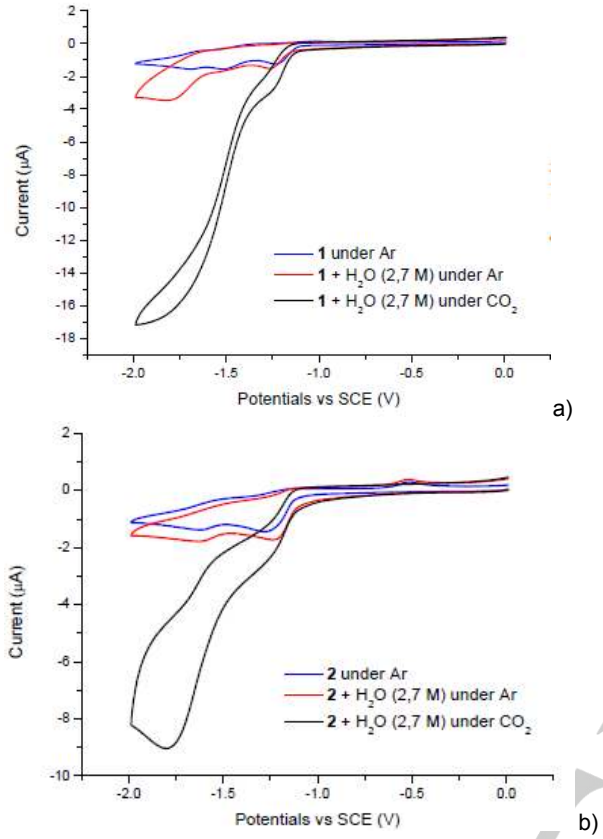

Figure 9. CVs at 100 mV s^{-1} of 0.5 mM MeCN solutions of **1** and **2** under Ar (blue), under Ar and with H_2O 2.7 M (red) and under CO_2 and with H_2O 2.7 M (black).

The presence of stronger Brønsted acids like TFE and phenol highlighted important differences in the product distribution of **1** and **2**. Unlike catalyst **2**, which remains basically selective towards CO production regardless of the acid employed, **1** exhibits a much more pronounced acid-dependent change in selectivity. In particular, in the presence of TFE, CO is still found as the major product (η_{CO} = 48%, TON_{CO} = 11) (Figure S17c), whereas the catalytic production of $HCOO^-$ increases significantly (η_{HCOO} = 36%, TON_{HCOO} = 9), giving an almost 1:1 CO/$HCOO^-$ ratio. In these conditions, H_2 is still produced in negligible quantities (η_{H2} = 3%, TON_{H2} = 0.8). This trend is amplified upon using an even stronger Brønsted acid like phenol (2.7 M), leading to $HCOO^-$ as the major product (η_{HCOO} = 39%, TON_{HCOO} = 12) and to CO in minor quantities (η_{CO} = 15%, TON_{CO} = 4). At the same time, H^+ reduction becomes significant (η_{H2} = 21% TON_{H2} = 5.5, Figure S18). Under the same experimental conditions, the catalytic selectivity of **2** is found to be less sensitive to the strength of the added acid than **1**. In particular, the electrocatalytic reduction of CO_2 to CO is still the main process, giving η_{CO} = 74% (TON_{CO} = 2, Figure S17d) and 56% (TON_{CO} = 2, Figure S19) at –1.70 V with 2.7 M TFE and phenol, respectively. $HCOO^-$ is formed in minor amounts, with η_{HCOO} = 10% (TON_{HCOO} = 0.3 with TFE) and 15% (TON_{HCOO} = 0.8 with phenol). Finally, bulk electrolysis in MeCN + 2.7 M TFE also produced traces of molecular hydrogen by using **2** as a catalyst (η_{H2} = 1%, TON_{H2} = 0.04), and in higher quantities when phenol is employed as external proton source (η_{H2} = 17%, TON_{H2} = 0.9).

Conclusions

In order to shed light on the influence of a ligand-centered proton relay on the CO_2 electroreduction catalyzed by tricarbonyl Mn diimine complexes, the electrochemical and spectroscopic features of the complexes **1** and **2** were systematically investigated under inert atmosphere as well as under CO_2. In particular, the results here presented highlight that how little modification in the position of the bpy-localized phenolic groups (in *ortho* for **1** and in *meta/para* for **2**) is able to produce substantial differences in the reductive mechanism under Ar, even inducing a different reactivity towards CO_2. Moreover, the selectivity dependence for the electrocatalytic CO_2 reduction process upon the strength of the external proton source was investigated in the presence of three different added acids (H_2O, TFE, phenol).

Taken together, CV and UV-Vis/IR-SEC data gave evidence of different electrochemical mechanisms for **1** and **2** under Ar. A fast Br^- dissociation of **1** at zero applied potential produces the acetonitrile complex **1a** as the main starting species in solution, whose 1e reduction does not lead to dimer formation but rather occurs via a reductive deprotonation process. As a result, the neutral intermediate **1b** is proposed as the main species formed after R1, in agreement with the experimental and DFT results. Furthermore, spectroscopic evidence of small amounts of a Mn hydride (**1c**) is found after the first reduction, being related to the OH proximity to the Mn center. No traces of such hydride species are detected under CO_2 atmosphere. IR-SEC under CO_2 in dry MeCN qualitatively well reproduces the quantitative loss of selectivity highlighted during bulk electrolysis, providing a mixture of CO and $HCOO^-$.[17] Notably, the well-known proton-independent mechanism of CO_2 disproportionation to CO and CO_3^{2-} cannot be ruled out under these conditions, as carbonate and bicarbonate anions are spectroscopically observed.

On the other hand, the electrochemical reduction of **2** under Ar follows the general scheme commonly reported for other [Mn(bpy-R_2)$(CO)_3$Br] catalysts, indicating that dimerization occurs upon R1'. Only traces of another Mn hydride species (**2c**) are detected after R1' in the absence of CO_2, but not under CO_2-saturated conditions. Moreover, IR-SEC of **2** under CO_2 confirmed a non-selective CO_2 reduction process in anhydrous MeCN, as well as a reduced electrocatalytic activity in comparison with **1**. Since pdbpy and ptbpy display similar bulkiness, the deviation between the electrochemical behavior of **1** and **2** are consistent with the differences in the proximity of the local proton source from the metal site and in the acidity of the ligand moiety.

Finally, controlled-potential electrolysis with different acids confirms the existence of competing electrocatalytic pathways,

leading to CO_2 conversion to CO and $HCOO^-$, in a ratio which is highly dependent on the acidity of the solution. Whereas the five-coordinate anions (e.g. **1d**, **1f**, **2d**) are likely responsible for the catalytic CO production, the $HCOO^-$ formation is supposed to be catalyzed by the transient Mn hydride species (**1c**, **2c**). Notably, addition of water (2.7 M) leads to selective CO_2 reduction to CO by both **1** and **2**, but side $HCOO^-$ and H_2 productions become more prominent as the strength of the Brønsted acid increases. Accordingly to these experimental data, acids stronger than water are able to give a fast reprotonation of the ligand-centered phenolate groups, favoring the *in-situ* formation of transient hydride species. Going from added water to phenol, the $CO:HCOO^-$ ratio can be tuned from *ca.* 23:1 to 1:3 with **1** as catalyst. In the case of **2**, such trend is much less evident than for **1** and this may be explained by a slower intramolecular proton transfer to form the catalytically active hydride. We believe that these findings contribute to a better understanding of the factors that control the selectivity of a promising class of earth-abundant transition metal catalysts.

Experimental Section

General considerations

NMR spectra were recorded on a JEOL EX 400 spectrometer (^{1}H operating frequency 400 MHz) at 298 K. ^{1}H and ^{13}C chemical shifts are reported relative to TMS (δ = 0) and referenced against solvent residual peaks. UV-Vis spectra were recorded in the 190-1100 nm range on an Agilent 8453 spectrophotometer. Infrared spectra were recorded in the 4000-1000 cm^{-1} range (with a resolution 2 cm^{-1}) on a Nicolet iS50 FT-IR spectrometer equipped with a KBr beam splitter and an MCT/A detector. The microanalysis samples were dried under vacuum to constant weight (20°C, *ca.* 0.1 Torr). Elemental analyses (C, H, N) were performed on a Fisons Instruments 1108 CHNS-O Elemental Analyzer. Tetrabutyl-ammonium hexafluorophosphate ($TBAPF_6$, Sigma-Aldrich, 98%) was recrystallized twice from ethanol and dried before use. All reagents were purchased from Sigma-Aldrich and used as received. Solvents were freshly distilled and purged with argon before use. All Mn complexes under study were carefully protected from light during use. Syntheses of the precursor (*E*)-picolinoyl-phenyl-ethene (a) and **1** have previously been reported.[17]

Synthesis of 1-(2-oxo-2-(3,4,5-trimethoxyphenyl)ethyl)pyridinium iodide (b): 20 mmol of 3′,4′,5′-trimethoxyacetophenone and 24 mmol of iodine were refluxed for 3 hours in 50 ml of pyridine. The reaction mixture was cooled to 0° C and the yellow product was precipitated, filtered and washed with cold pyridine (yield 80%).[31] ^{1}H-NMR [400 MHz, $(CD_3)_2CO$]: δ/ppm = 9.36 (d, *J* = 5.8 Hz, 2H), 8.89 (t, *J* = 7.9 Hz,1H), 8.40 (t, *J* = 7.0 Hz, 2H), 7.50 (s, 2H), 7.07 (s, 2H), 3.96 (s, 6H), 3.85 (s, 3H).

Synthesis of 4-phenyl-6-(3,4,5-trimethoxyphenyl)-2,2'-bipyridine (c): 2.8 mmol of (a) and an equivalent amount of (b) were added to a flask with an excess of ammonium acetate (28 mmol) and 20 ml of methanol. The mixture was purged with Ar for ten minutes and was then heated to reflux for 6 hours. The solution was dried on vacuum and the solid was dissolved in 30 ml of ethyl acetate. The organic phase was washed three times using an aqueous solution of $NaHCO_3$ (10%) and then dried using anhydrous $MgSO_4$. The solid collected after removal of the solvent was purified on a silica gel column (petroleum ether/ethyl acetate 7:1; yield: 40%).[32] ^{1}H-NMR (400 MHz, $(CD_3)_2CO$): δ/ppm = 8.73-8.67 (m, 2H), 8.42 (s, 1H), 8.26 (d, J= 7.3 Hz, 2H), 7.98 (t, *J* = 7.9 Hz, 1H), 7.86 (s, 1H), 7.53 (t, *J* = 7.7 Hz, 2H), 7.47-7.41 (m, 2H), 6.41 (s, 2H), 3.90 (s, 3H), 3.78 (s, 6H).

Synthesis of 4-phenyl-6-(3,4,5-trihydroxyphenyl)-2,2'-bipyridine (ptbpy): 0.9 mmol of (c) was added to a solution of HBr (33%) in acetic acid and heated to reflux for 72 hours. The mixture was then cooled to room temperature and neutralized using an aqueous solution of NaOH. The green precipitate was filtered and washed with water and chloroform (yield 93%). ^{1}H-NMR (400 MHz, d_6-DMSO): δ/ppm = 9.14 (s, 2H), 8.73 (d, *J* = 4.7 Hz, 1H), 8.58-8.56 (m, 2H), 8.48 (s, 1H), 8.03 (td, ^1J = 7.9 Hz, ^2J = 1.4 Hz, 1H), 7.98 (s, 1H), 7.92 (d, 7.3 Hz, 2H), 7.58 (t, *J* = 7.6 Hz, 2H), 7.53-7.49 (m, 2H), 7.31 (s, 2H). ^{13}C-NMR (400 MHz, d_6-DMSO): δ/ppm = 156.97, 155.59, 155.44, 149.50, 149.39, 146.39, 138.05, 137.54, 135.15, 129.47, 128.99, 127.16, 124.55, 120.84, 117.04, 115.63, 106.20. MS (ESI^+): *m/z* = 357.28 $[M\text{-}H]^+$.

Synthesis of [Mn(ptbpy)(CO)$_3$Br] (2): $Mn(CO)_5Br$ (1 eq) and ptbpy (1.01 eq) were refluxed for 4 hours in diethyl ether under stirring. The reaction mixture was then cooled to room temperature and the orange product was filtered and washed once with diethyl ether (yield 82%). ^{1}H-NMR (400 MHz, $(CD_3)_2CO$): δ/ppm = 9.31 (d, *J* = 4.7 Hz, 1H), 8.83-8.79 (m, 2H), 8.40-8.14 (m, 3H), 8.08 (d, *J* = 6.2 Hz, 2H), 7.90 (s, 1H), 7.76-7.71 (m, 2H), 7.58 (m, 3H), 6.75 (s, 2H). ^{13}C-NMR (400 MHz, $(CD_3)_2CO$): δ/ppm = 166.81, 158.66, 157.56, 153.96, 150.73, 146.69, 139.45, 136.91, 135.65, 135.00, 131.14, 130.20, 128.43, 126.73, 125.37, 124.71, 119.56, 109.87, 109.78. IR (ATR): 3499, 3306, 2032, 1963, 1912 cm^{-1}. MS (ESI^+): *m/z* = 573.08, 575.02 $[M\text{-}H]^+$.

Electrochemistry

All the solvents used for electrochemical experiments were freshly distilled. Cyclic voltammetry experiments were performed using a Metrohm Autolab 302N potentiostat. 0.5-1.0 mM solutions of the compounds were used in MeCN, with tetrabutylammonium hexafluorophosphate ($TBAPF_6$) as the supporting electrolyte (0.1 M). A single-compartment cell, with a glassy carbon (GC) working electrode (Ø = 1 mm) was employed, while a Pt counter electrode and a SCE (KCl 3M) reference electrode were also used. In our experimental conditions, the reference ferrocene/ferrocinium (Fc/Fc^+) redox is at $E_{1/2}$ = 0.39 V (ΔE_p = 65 mV). The Ar- and CO_2-saturated conditions were achieved by purging gases for 5 minutes before each potential sweep.

Spectroelectrochemistry

IR-SEC experiments were performed using the optically transparent thin-layer electrode (OTTLE) cell, equipped with a Pt minigrid working and auxiliary electrodes, an Ag microwire pseudo reference electrode and a CaF_2 window.[33] IR spectra were recorded on a Nicolet iS50 FT-IR spectrometer. UV-Vis spectroelectrochemistry was performed using the OTTLE cell equipped with quartz optical windows and spectra were measured with diode-array spectrometer Agilent 8453. The course of spectroelectrochemical experiments was controlled and monitored using a PA4 potentiostat and recorder (Laboratory Devices, Prague, Czech Republic). $TBAPF_6$ was used as the supporting electrolyte during the experiments.

Controlled-potential electrolysis

A double compartment H-type cell was used with a Pt wire as the counter electrode in a bridge separated from the cathodic compartment by a glass frit. A glassy carbon rod was used as the working electrode along with an aqueous SCE reference electrode. CPE experiments were

performed in acetonitrile with 0.1 M $TBAPF_6$ as the supporting electrolyte and 0.5 mM of the catalysts **1** and **2** at –1.5 V and –1.7 V *vs.* SCE, respectively. The acids H_2O, TFE and phenol were added to the solution in equimolar quantity (2.7 M). A controlled flow of CO_2 (50 mL min^{-1}), measured just before arrival into the cell, was maintained during the CPE measurements by means of a Smart Trak 100 (Sierra) flow controller. All the electrochemical cells were airtight and equipped with a bubbler that maintained the inner atmosphere but avoided gas overpressure.

Quantitative analysis of CO_2 reduction products

CO and H_2 were detected and quantified using an Agilent 490 Micro GC gas chromatograph equipped with a Molsieve 5 Å column, which was kept at 90° C and a pressure of 200 kPa, and a thermal conductivity detector. The carrier gas was Ar. The gas inside the measurement cell was sampled for 90s every five minutes and fill the Micro GC 10 µL sample loop, and eventually 500 nL were injected into the column for the analyses. It was possible to determine the amounts of CO and H_2 produced during the experiment from the concentrations of CO and H_2 in the gas samples and knowledge of the gas flow and the cell volume. We used Ar, He, N_2, O_2, CO_2 and CO pure gases (>99.9995%), from Sapio, for the operation and calibration of the flow controller and GC apparatus, while H_2 was produced using a Claind HyGen hydrogen generator. The detection limits for CO and H_2 were 20 ppmv and 0.5 ppmv respectively. Formic acid production was evaluated using ion chromatography; specifically, a Dionex DX 500 instrument equipped with a Dionex IonPac® AS9-HC column (200 mm × 4 mm i.d.), GP40 pump (Dionex), an electrochemical detector ED40 (Dionex) and an Anion Self-Regenerating Suppressor-Ultra (ARSR®-ULTRA, 4-mm, Dionex). Elution was performed in isocratic conditions with an aqueous solution of K_2CO_3 9.0 10^{-3} M at 0.70 mL min^{-1} flow rate. We observed a retention time of 6.23 min for the formate anion in these conditions. The $TBAPF_6$ matrix had to be removed for the analysis. Therefore, the samples were filtered and brought to 25.0 mL in volumetric flasks after basification with ammonia. We then injected 2.00 mL of each sample into a disposable SPE column (containing BAKERBOND spe™ Quaternary Amine (N+) and Carlo Erba Amberlite® CG-120, previously conditioned with HCl 0.01 M) and eluted with 8.00 mL of HCl 0.010 M. The resulting solutions were brought to pH = 12 using NaOH 2 M and analyzed by means of ion chromatography.

Computational Details

DFT calculations were performed using Gaussian 09 Rev. D.01,[34] including the solvent effect by the conductor-like polarizable continuum model (CPCM)[35] with acetonitrile as solvent. Geometry optimizations were carried out without any constraints using the B3LYP functional,[36] the optimized def2-TZVP basis set for Mn and Br and the def2-SVP basis set[37] for all other atoms. The D3 version of Grimme's dispersion method was applied adopting the Becke-Johnson damping scheme.[38] Gibbs Free Energies were determined by thermal corrections for entropy and enthalpy at 298 K to the electronic energies. In these calculations, the computed harmonic frequencies were scaled by 0.952 to account for anharmonicity. For radical anions, unrestricted Kohn–Sham formalism (UKS) was adopted. The nature of all stationary points were confirmed by normal-mode analysis (no imaginary frequencies were found).

Acknowledgements

Financial support from project PHOTORECARB (Progetti di Ateneo/CSP 2012, Call 03, Università di Torino & Compagnia Sanpaolo) is gratefully acknowledged. J.F. thanks the Grant Agency of the Czech Republic (grant 14-05180S) for support.

Keywords: carbon dioxide • manganese • electrochemistry • DFT calculations • electrocatalysis

[1] a) J. Qiao, Y. Liu, F. Hong, J. Zhang, *Chem. Soc. Rev.* **2014**, *43*, 631-675; b) J. Ronge, T. Bosserez, D. Martel, C. Nervi, L. Boarino, F. Taulelle, G. Decher, S. Bordiga, J. A. Martens, *Chem. Soc. Rev.* **2014**, *43*, 7963-7981.

[2] a) C. Costentin, S. Drouet, M. Robert, J. M. Saveant, *Science* **2012**, *338*, 90-94; b) C. Costentin, G. Passard, M. Robert, J. M. Saveant, *Proc. Natl. Acad. Sci* **2014**, *111*, 14990-14994; c) C. Costentin, M. Robert, J.-M. Savéant, A. Tatin, *Proc. Natl. Acad. Sci.* **2015**, *112*, 6882–6886.

[3] a) I. Wender, *Fuel Process. Technol.* **1996**, *48*, 189–297; b) M. Dry, E. *Catal. Today* **2002**, *71*, 227-241.

[4] C. Rice, S. Ha, R. I. Masel, P. Waszczuk, A. Wieckowski, T. Barnard, *J. Power Sources* **2002**, *111*, 83–89.

[5] A. S. Agarwal, Y. Zhai, D. Hill, N. Sridhar, *ChemSusChem* **2011**, *4*, 1301–1310.

[6] a) J. Hawecker, J.-M. Lehn, R. Ziessel, *J. Chem. Soc. Chem. Commun.* **1984**, *984*, 328; b) J. W. Raebiger, J. W. Turner, B. C. Noll, C. J. Curtis, A. Miedaner, B. Cox, D. L. Dubois, N. Renewable, C. B. V, N. Dame, et al., *Organometallics* **2006**, *25*, 3345–3351; c) Z. Chen, C. Chen, D. R. Weinberg, P. Kang, J. J. Concepcion, D. P. Harrison, M. S. Brookhart, T. J. Meyer, *Chem. Commun.* **2011**, *47*, 12607; d) J. D. Froehlich, C. P. Kubiak, *J. Am. Chem. Soc.* **2015**, *137*, 3565–3573.

[7] a) C. M. Bolinger, B. P. Sullivan, D. Conrad, J. A. Gilbert, N. Story, T. J. Meyer, *J. Chem. Soc. Commun.* **1985**, 796–797; b) H. Ishida, H. Tanaka, K. Tanaka, T. Tanaka, *J. Chem. Soc. Chem. Commun.* **1987**, 131; c) C. Arana, S. Yan, M. Keshavarz-K., K. T. Potts, H. D. Abruna, *Inorg. Chem.* **1992**, *31*, 3680–3682; d) A. Taheri, E. J. Thompson, J. C. Fettinger, L. A. Berben, *ACS Catal.* **2015**, *5*, 7140–7151; e) L. Chen, Z. Guo, X. G. Wei, C. Gallenkamp, J. Bonin, E. Anxolabéhère-Mallart, K. C. Lau, T. C. Lau, M. Robert, *J. Am. Chem. Soc.* **2015**, *137*, 10918–10921; f) P. Kang, C. Cheng, Z. Chen, C. K. Schauer, T. J. Meyer, M. Brookhart, *J. Am. Chem. Soc.* **2012**, *134*, 5500–5503; g) P. Kang, S. Zhang, T. J. Meyer, M. Brookhart, *Angew. Chem. Int. Ed.* **2014**, *53*, 8709–8713.

[8] a) M. Bourrez, F. Molton, S. Chardon-Noblat, A. Deronzier, *Angew. Chem. Int. Ed.* **2011**, *50*, 9903–9906; b) J. M. Smieja, M. D. Sampson, K. A. Grice, E. E. Benson, J. D. Froehlich, C. P. Kubiak, *Inorg. Chem.* **2013**, *52*, 2484–2491; c) F. Franco, C. Cometto, C. Garino, C. Minero, F. Sordello, C. Nervi, R. Gobetto, *Eur. J. Inorg. Chem.* **2015**, *2015*, 296–304; d) F. Franco, C. Cometto, F. Sordello, C. Minero, L. Nencini, J. Fiedler, R. Gobetto, C. Nervi, *ChemElectroChem* **2015**, *2*, 1372–1379; e) M. D. Sampson, C. P. Kubiak, *J. Am. Chem. Soc.* **2016**, *138*, 1386–1393.

[9] a) F. Hartl, B. D. Rossenaar, G. J. Stor, D. J. Stufkens, *Recl. des Trav. Chim. des Pays-Bas* **2010**, *114*, 565–570; b) F. P. A. Johnson, M. W. George, F. Hartl, J. J. Turner, *Organometallics* **1996**, *15*, 3374–3387; c) C. W. Machan, M. D. Sampson, S. A. Chabolla, T. Dang, C. P. Kubiak, *Organometallics* **2014**, *33*, 4550–4559; d) Q. Zeng, J. Tory, F. Hartl, *Organometallics* **2014**, *33*, 5002–5008.

[10] E. E. Benson, M. D. Sampson, K. A. Grice, J. M. Smieja, J. D. Froehlich, D. Friebel, J. A. Keith, E. A. Carter, A. Nilsson, C. P. Kubiak, *Angew. Chem. Int. Ed.* **2013**, *52*, 4841–4844.

[11] M. Bourrez, M. Orio, F. Molton, H. Vezin, C. Duboc, A. Deronzier, S. Chardon-Noblat, *Angew. Chem. Int. Ed.* **2014**, *53*, 240–243.

[12] D. C. Grills, J. Farrington, B. H. Layne, S. V. Lymar, B. A. Mello, J. M. Preses, J. F. Wishart, *J. Am. Chem. Soc.* **2014**, *136*, 5563–5566.

[13] a) J. a. Keith, K. a. Grice, C. P. Kubiak, E. a. Carter, *J. Am. Chem. Soc.*

2013, *135*, 15823–15829; b) C. Riplinger, M. D. Sampson, A. M. Ritzmann, C. P. Kubiak, E. A. Carter, *J. Am. Chem. Soc.* **2014**, *136*, 16285–16298; c) C. Riplinger, E. A. Carter, *ACS Catal.* **2015**, *5*, 900–908.

[14] E. E. Benson, C. P. Kubiak, *Chem. Commun.* **2012**, *48*, 7374–6.

[15] M. D. Sampson, A. D. Nguyen, K. A. Grice, C. E. Moore, A. L. Rheingold, C. P. Kubiak, *J. Am. Chem. Soc.* **2015**, *137*, 3718.

[16] We assume that protons were taken from solvent to reprotonate the catalyst.[17] The terms *anhydrous* and *dry* will be used to indicate freshly distilled organic solvents (thoroughly used for all electrochemical experiments), without added Brønsted acids.

[17] F. Franco, C. Cometto, F. Ferrero Vallana, F. Sordello, E. Priola, C. Minero, C. Nervi, R. Gobetto, *Chem. Commun.* **2014**, *50*, 14670–3.

[18] H. Takeda, H. Koizumi, K. Okamoto, O. Ishitani, *Chem. Commun.* **2014**, *50*, 1491–3.

[19] H. Fei, M. D. Sampson, Y. Lee, C. P. Kubiak, S. M. Cohen, *Inorg. Chem.* **2015**, *54*, 6821–6828.

[20] J.-D. Compain, M. Bourrez, M. Haukka, A. Deronzier, S. Chardon-Noblat, C. Costentin, M. Robert, J. M. Saveant, B. Kumar, M. Llorente, et al., *Chem. Commun.* **2014**, *50*, 2539.

[21] J. J. Walsh, C. L. Smith, G. Neri, G. F. S. Whitehead, C. M. Robertson, A. J. Cowan, *Faraday Discuss.* **2015**, *183*, 147–160.

[22] J. Agarwal, T. W. Shaw, H. F. Schaefer, A. B. Bocarsly, *Inorg. Chem.* **2015**, *54*, 5285–5294.

[23] G. F. Manbeck, J. T. Muckerman, D. J. Szalda, Y. Himeda, E. Fujita, *J. Phys. Chem. B* **2015**, *119*, 7457–7466.

[24] F. J. Garcia Alonso, A. Llamazares, V. Riera, M. Vivanco, S. Garcia Granda, M. R. Diaz, *Organometallics* **1992**, *11*, 2826–2832.

[25] a) K. A. Grice, N. X. Gu, M. D. Sampson, C. P. Kubiak, *Dalt. Trans.* **2013**, *42*, 8498; b) D. Osella, C. Nervi, M. Ravera, J. Fiedler, V. V. Strelets, *Organometallics* **1995**, *14*, 2501–2505.

[26] a) D. H. Gibson, X. L. Yin, H. Y. He, M. S. Mashuta, *Organometallics* **2003**, *22*, 337–346; b) M. D. Sampson, J. D. Froehlich, J. M. Smieja, E. E. Benson, I. D. Sharp, C. P. Kubiak, *Energy Environ. Sci.* **2013**, *6*, 3748–3755; c) T. Morimoto, T. Nakajima, *J. Am. Chem. Soc.* **2013**, *135*, 16825–16828.

[27] S. C. Cheng, C. A. Blaine, M. G. Hill, K. R. Mann, *Inorg. Chem.* **1996**, *2*, 7704–7708.

[28] J. Tory, B. Setterfield-Price, R. A. W. Dryfe, F. Hartl, *ChemElectroChem* **2015**, *2*, 213–217..

[29] P. Christensen, A. Hamnett, A. V. G. Muir, J. A. Timney, *J. Chem. Soc. Dalt. Trans* **1992**, 1455–1463.

[30] I. Azcarate, C. Costentin, M. Robert, J.-M. Savéant , *J. Phys. Chem. C* **2016**, *120*, 28951-28960.

[31] A. Basnet, P. Thapa, R. Karki, Y. Na, Y. Jahng, B.-S. Jeong, T. C. Jeong, C.-S. Lee, E.-S. Lee, *Bioorg. Med. Chem.* **2007**, *15*, 4351–4359.

[32] F. Neve, M. Ghedini, O. Francescangeli, S. Campagna, *Liq. Cryst.* **1998**, *24*, 673–680.

[33] M. Krejčik, M. Daněk, F. Hartl, *J. Electroanal. Chem. Interfacial Electrochem.* **1991**, *317*, 179–187.

[34] Frisch, M. J. et al Gaussian 09, Rev. D.01 **2009**.

[35] a) S. Miertus, E. Scrocco, J. Tomasi, *Chem. Phys.* **1981**, *55*, 117–129; b) M. Cossi, G. Scalmani, N. Rega, V. Barone, *J. Chem. Phys.* **2002**, *117*, 43–54.

[36] a) A. D. Becke, *J. Chem. Phys.* **1993**, *98*, 5648; b) C. Lee, W. Yang, R. G. Parr, *Phys. Rev. B* **1988**, *37*, 785–789.

[37] a) F. Weigend, R. Ahlrichs, *Phys. Chem. Chem. Phys.* 2005, *7*, 3297–305; b) F. Weigend, *Phys. Chem. Chem. Phys.* **2006**, *8*, 1057–1065.

[38] S. Grimme, S. Ehrlich, L. Goerigk, *J. Comput. Chem.* **2011**, *32*, 1456–1465.

WILEY-VCH

Entry for the Table of Contents

FULL PAPER

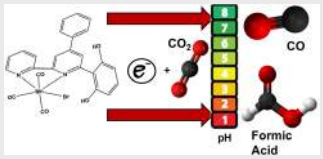

The electrochemical behavior of *fac*-[Mn(pdbpy)$(CO)_3$Br] (pdbpy = 4-phenyl-6-(phenyl-2,6-diol)-2,2'-bipyridine) in MeCN under Ar and its catalytic performances for CO_2 reduction with added water, TFE and phenol are discussed. Bulk electrolysis reveals that the process selectivity is sensitive to the acid strength, providing CO and formate in different faradaic yields. The key role of the local proton source is demonstrated by a detailed spectroelectrochemical study under Ar and CO_2.

Federico Franco, Claudio Cometto, Luca Nencini, Claudia Barolo, Fabrizio Sordello, Claudio Minero, Jan Fiedler, Marc Robert, Roberto Gobetto and Carlo Nervi**

Page No. – Page No.

Local Proton Source in the Electrocatalytic CO_2 Reduction by Mn(bpy-R)$(CO)_3$Br Complexes

WILEY-VCH